Linking satellites to genes with machine learning to estimate phytoplankton community structure from space

Roy El Hourany[1], Juan Pierella Karlusich[2,3], Lucie Zinger[2,4], Hubert Loisel[1], Marina Levy[5], and Chris Bowler[2]

[1]Univ. Littoral Côte d'Opale, Univ. Lille, CNRS, IRD, UMR 8187, LOG, Laboratoire d'Océanologie et de Géosciences, F 62930 Wimereux, France
[2]Institut de Biologie de l'Ecole Normale Supérieure (IBENS), Ecole Normale Supérieure, CNRS, INSERM, Université PSL, 75005 Paris, France
[3]FAS Division of Science, Harvard University, Cambridge, MA
[4]Naturalis Biodiversity Center, 2300 RA Leiden, The Netherlands
[5]Sorbonne Université, LOCEAN-IPSL, Laboratoire d'Océanographie et du Climat ; Expérimentations et Approches Numériques, CNRS, IRD, MNHN, 75005 Paris, France

Correspondence: Roy El Hourany (roy.elhourany@univ-littoral.fr), Marina Levy (marina.levy@locean.ipsl.fr), Chris Bowler (cbowler@biologie.ens.fr)

Abstract. Ocean color remote sensing has been used for more than two decades to estimate primary productivity. Approaches have also been developed to disentangle phytoplankton community structure based on spectral data from space, in particular when combined with in situ measurements of photosynthetic pigments. Here, we propose a new ocean color algorithm to derive the relative cell abundance of seven phytoplankton groups, as well as their contribution to total chlorophyll-a (Chla) at the global scale. Our algorithm is based on machine learning and has been trained using remotely-sensed parameters (reflectance, backscattering, and attenuation coefficients at different wavelengths, plus temperature and Chla) combined with an omics-based biomarker developed using *Tara* Oceans data representing a single-copy gene encoding a component of the photosynthetic machinery that is present across all phytoplankton, including both prokaryotes and eukaryotes. It differs from previous methods which rely on diagnostic pigments to derive phytoplankton groups. Our methodology provides robust estimates of the phytoplankton community structure in terms of relative cell abundance and contribution to total Chla concentration. The newly generated datasets yield complementary information about different aspects of phytoplankton that are valuable for assessing the contributions of different phytoplankton groups to primary productivity and inferring community assembly processes. This makes remote sensing observations excellent tools to collect Essential Biodiversity Variables and provide a foundation for developing marine biodiversity forecasts.

1 Introduction

The production of organic matter (i.e., productivity) in marine ecosystems relies largely on phytoplankton. These unicellular photosynthetic microorganisms are evolutionarily diverse and exhibit a wide range of cell morphologies, sizes, photosynthetic accessory pigments, elemental requirements, and biogeochemical and trophic functions (Pierella Karlusich et al., 2020). They

play a key role in regulating ocean biogeochemistry (Fuhrman, 2009) and global climate, partly through the absorption of atmospheric CO2 and export of carbon to the deep ocean (Guidi et al., 2009; Tilman et al., 2014; Tara Ocean Foundation, 2022).

In order to investigate the potential impacts of environmental changes on marine ecosystem functioning (Ibarbalz et al., 2019; Henson et al., 2021), high-resolution, real-time, and global scale data on phytoplankton community structure are required (Pereira et al., 2013). However, existing knowledge about the global distribution of phytoplankton communities from in-situ observations is highly fragmented, spatially disparate, and temporally punctual. It is furthermore limited by both the challenges of in situ data collection and by the associated costs of measurement techniques, which range from microorganism imaging, flow cytometry, to DNA sequencing (Hillebrand and Azovsky, 2001; Irigoien et al., 2004; Smith, 2007; Rodríguez-Ramos et al., 2015; Powell and Glazier, 2017; Righetti et al., 2019; Dutkiewicz et al., 2020; Pierella Karlusich et al., 2020).

Ocean color remote sensing offers an interesting alternative to map the global distribution of phytoplankton communities at the sea surface at a high spatio-temporal resolution. Since 1978, ocean color satellites have been used to observe the concentration of the main phytoplankton pigment, chlorophyll-a (Chla), considered as a proxy of phytoplankton biomass (O'Reilly et al., 1998; Sathyendranath et al., 2014). Recently, ocean color data have also been used to gain information about phytoplankton communities, such as their size structure, and their taxonomic or functional composition. This interest has facilitated the integration of the concept of phytoplankton functional types (PFT) into studies of a range of ecological and biogeochemical problems (Le Quéré et al., 2005; Hood et al., 2006). Functional types correspond to categories linked to biogeochemical processes (e.g., silicifiers, calcifiers) and physiological adaptations to environmental factors (e.g., light, nutrients, turbulence), or to more practical categories quantified using a particular analytical technique (e.g., pigment types) (IOCCG report N 14). Specialized algorithms applied to ocean color data have consequently been developed to detect specific taxa with distinctive optical characteristics (Brown, 1995; Iglesias-Rodríguez et al., 2002), or the abundance of phytoplankton functional types and size classes (Alvain et al., 2005; Uitz et al., 2006; Aiken et al., 2009; Bracher et al., 2009; Hirata et al., 2011; Chase et al., 2020; Ben Mustapha et al., 2013; Alvain et al., 2008).

The diagnostic pigment analysis method (DPA, Vidussi et al. (2001)) relies on the association of secondary phytoplankton pigments with different broad taxonomic phytoplankton groups. DPA classification was later refined by Uitz et al. (2006) who gave different weightings to the diagnostic pigments to retrieve three phytoplankton size classes (PSC) from total Chla. The advantage of this method is that phytoplankton pigments can be measured in a cost-effective manner through high performance liquid chromatography (HPLC). Today, large in-situ HPLC datasets are available with broad spatial and temporal coverage. These HPLC datasets have enabled the development of several DPA-based ocean color algorithms, which has made it possible to evaluate the abundance of different phytoplankton groups and size classes from ocean color satellite data (Uitz et al., 2006; Hirata et al., 2008, 2011; Soppa et al., 2014; Di Cicco et al., 2017; Organelli et al., 2013; El Hourany et al., 2019a, b; Xi et al., 2020) . However, the limitation of the DPA approach is that it is associated with large uncertainties in the classification of phytoplankton due to the presence of certain pigments in different phytoplankton taxa and cell size classes, which also vary with acclimation to light, temperature, and nutrient availability (Brewin et al., 2014; Chase et al., 2020).

In this work, we propose an alternate approach to develop an ocean color algorithm for phytoplankton group detection from in-situ metagenomic observations. The approach is ground-truthed on data collected by *Tara* Oceans, which constitutes the most comprehensive and harmonized molecular dataset available on phytoplankton taxonomic community structure on a global scale. More specifically, we used metagenomics reads to extract the global-scale distribution and abundance of the single-copy gene psbO, which is present across all phytoplankton groups and that provides an unbiased picture of phytoplankton cell abundances (Pierella Karlusich et al., 2022). We used these data, together with satellite-derived optical, physical and biogeochemical parameters to train an unsupervised machine learning algorithm able to discern the non-linear relationship between phytoplankton taxonomic community structure and data derived from satellites. This new algorithm allowed us to derive the spatio-temporal variability of seven phytoplankton groups between 1997 and 2021. We then compared the performance of this new algorithm with that of two previous DPA-based algorithms (El Hourany et al., 2019a; Xi et al., 2020).

2 Materials

In this section, we present the datasets that were used for training the algorithm and for evaluating the outputs. The input dataset includes the in-situ distribution and abundance of phytoplankton groups inferred from metagenomics data from *Tara* Oceans and their associated satellite matchups. The outputs of the new algorithm are compared to a global dataset of in-situ HPLC diagnostic pigments, as well as with estimates from two DPA-based remote sensing algorithms.

2.1 Input dataset

2.1.1 Metagenomic read abundance of the *psbO* gene

The *psbO* gene encodes the manganese-stabilizing protein, of around 270 amino acids, which constitutes a core subunit of photosystem II (PSII) and is unique to organisms carrying out oxygenic photosynthesis. The *psbO* gene is a single-copy gene in the vast majority of eukaryotes and prokaryotes. We used *psbO* reads from the metagenomes generated from the *Tara* Oceans expedition as a proxy of phytoplankton relative cell abundance (Pierella Karlusich et al., 2022). Among the 211 *Tara* Oceans stations, 145 stations sampled *psbO* reads in different ocean regimes from oligotrophic to eutrophic waters (Chla from 0.01 to 10 $mg.m^{-3}$, median at 0.3 $mg.m^{-3}$), from 2009 to 2013. Seawater samples were filtered in order to differentiate five planktonic size fractions (0.22-3um, 0.8-5um, 5-20um, 20-180 um, 180-2000 um). For the purpose of this study, we pooled the five size fractions into a single aggregated sample, correcting by the different sampling volumes for each size fraction, and discarded stations where not all size fractions were available, to avoid biasing the results.

psbO data enabled us to taxonomically differentiate seven phytoplankton groups: diatoms, dinoflagellates, green algae, haptophytes, pelagophytes, cryptophytes, and prokaryotes (Cyanobacteria) (Fig. 1). The *psbO* read abundances of these seven groups are expressed as relative phytoplankton cell abundance (%). Phytoplankton that were not assigned to any of these seven groups (Unclassified) represented less than 5% of the total phytoplankton community.

In addition to the use of *psbO* as a proxy of relative cell abundance, we also estimated the Chla proportion of the most abundant phytoplankton groups. For this, the relative *psbO* read abundances were weighted by their size fraction and then multiplied by the in-situ value of Chla measured at each *Tara* Oceans station. This conversion from *psbO* reads to Chla gives the contribution of each phytoplankton group to the total Chla, by accounting for cell size. We should note however that filters may retain cells smaller than the nominal pore size because of net clogging, being trapped in fecal pellets, as well as being present as symbioses and colonies. This has been observed with prokaryotic pico-sized cells such as Synechococcus and Prochloroccocus being over-represented in the 180-2000 um size fraction (Fig. 2). To minimize this impact, we based our size-weighting on 4 size-fractions, while excluding the 180-2000 um size range following the protocol in Sommeria-Klein et al., 2021. Chla fraction per group is expressed as follows:

$$\text{Chla fraction}_{\text{PFT}} = \frac{\text{Chla}_{\text{in-situ}} \cdot \left(\sum_{s=1}^{4} (\text{psbO}_{\text{PFT}} \cdot \text{size}_s) \right)}{\sum_{s=1}^{4} \sum_{\text{PFT}=1}^{7} (\text{psbO}_{\text{PFT}} \cdot \text{size}_s)}$$

where PFT is a designated phytoplankton group, and size is the four used size fractions.

There are hence two levels of information derived from the molecular dataset; relative abundance of *psbO* reads as a proxy of relative cell abundance, and the fraction of Chla that each group represents. Both types of information have different implications. Chla is often used as a proxy of biomass, which is a relevant parameter for energy and matter fluxes (e.g., food webs, biogeochemical cycles), while cell abundance corresponds to species abundance for unicellular organisms, which is an important measure for inferring community assembly processes.

2.1.2 Satellite datasets

We used ocean color products from the Globcolour project (R2019, full archive reprocessed, 2020) from 1997 to the present day, downloaded from the Globcolour portal. These products were constructed by merging data from various satellite sensors: Sea-viewing Wide Field-of-view Sensor (SeaWiFS), Moderate Resolution Imaging Spectroradiometer (MODIS), Visible Infrared Imaging Radiometer Suite (VIIRS), Medium Resolution Imaging Spectrometer (MERIS), and Ocean and Land Colour Instrument (OLCI). We used sixteen Globcolour products: Chlorophyll-a concentration (Chla, product name: CHL1-AVW), Remote sensing reflectances (Rrs) at 11 wavelengths (412 till 670 nm), light attenuation coefficient at 490 nm (Kd490), photosynthesis available radiation (PAR), Normalized fluorescence light height (NFLH) and particulate backscattering at 443 nm (bbp). These products have daily and 4km spatio-temporal resolution. In addition, we used the Climate Change Initiative Sea Surface Temperature (SST) product at 4 km resolution and daily frequency distributed by the Copernicus Marine Services (CMEMS) portal.

2.2 HPLC datasets

To compare *psbO*-derived phytoplankton group distributions with more conventional, DPA-based products, we compiled a global HPLC dataset regrouping 12 000 HPLC observations from several HPLC datasets between 1997 and 2014 (Fig. 3):
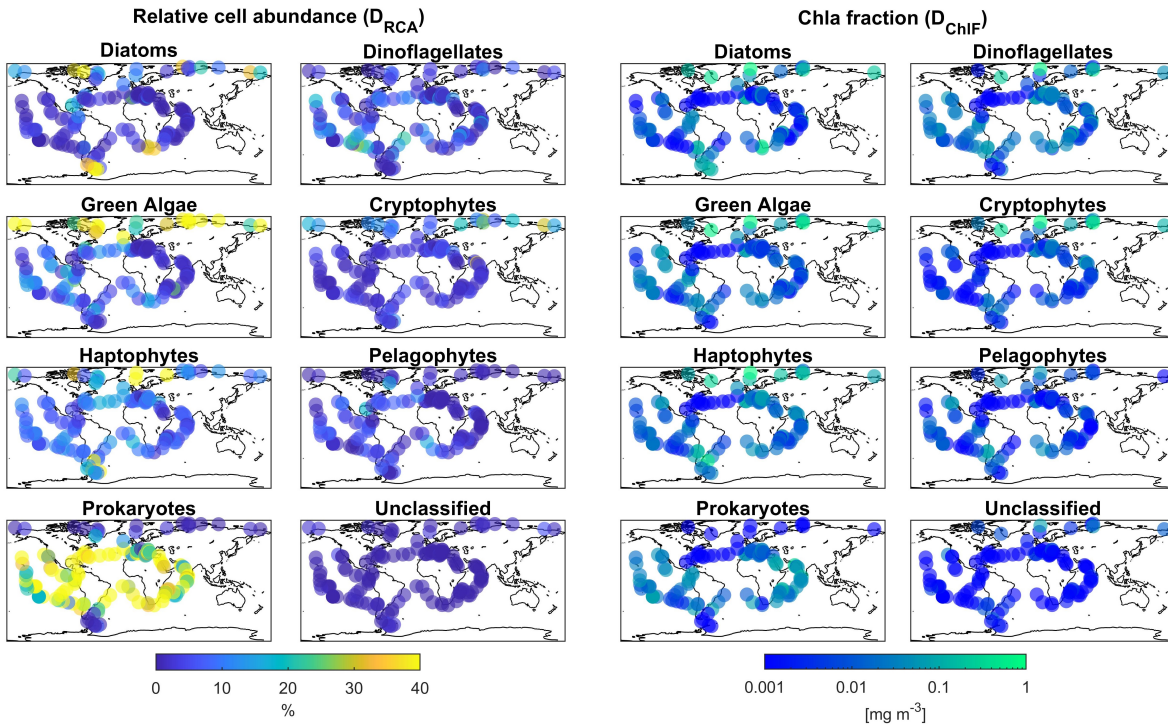
Figure 1. Global biogeographical patterns of marine phytoplankton relative cell abundance and Chla fraction per group based on *psbO* reads obtained from metagenomes from seawater samples collected during the *Tara* Oceans expeditions.
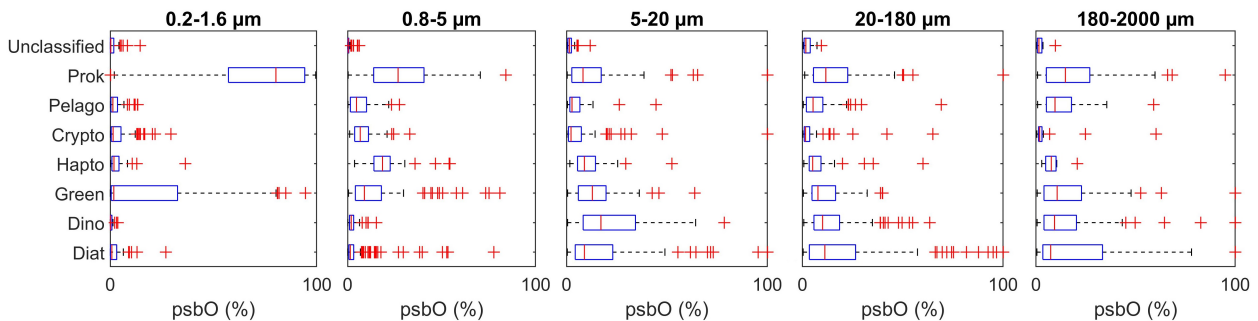

Figure 2. Relative abundance of *psbO* reads as a proxy of phytoplankton group cell abundance observed in each size fraction. The boxplots represent the distribution of each group and each panel shows the different size fractions.

MAREDAT, NOMAD, SeaBASS, and other oceanographic campaigns: Labrador, Gep&co, Polarstern, BROKE-West, SAZ-Sense Voyage (Luo et al., 2012; Werdell and Bailey, 2005; Dandonneau et al., 2004; Bracher et al., 2015; Fragoso et al., 2016; Peloquin et al., 2013; Wright et al., 2010; de Salas et al., 2011). This HPLC dataset was collocated with satellite Globcolor and CCI matchups. It depicts the abundance of the pigments most widely used to identify major phytoplankton groups: Fucoxanthin

(Fuco), Peridinin (Perid), Alloxanthin (Allo), Zeaxanthin (Zea), Chlorophyll-b (Chlb), 19'-Hexanoyloxyfucoxanthin (19HF), and 19'-Butanoyloxyfucoxanthin (19BF) (Table 1). To estimate Chla fraction for each phytoplankton group, namely diatoms, dinoflagellates, haptophytes, green algae, cryptophytes, pelgophytes and prokaryotes, diagnostic pigments were used. The Chla fraction per group is expressed by:

$$\text{Chla}_{\text{PFT}} = \frac{DP \cdot \alpha}{\sum DP \cdot \alpha}$$

where a is a coefficient associated with a diagnostic pigment (DP) for a specific PFT.

Three sets of coefficients a are proposed for a global ocean application and are presented in Table 1 (Uitz et al., 2006; Soppa et al., 2014; Brewin et al., 2015). Therefore we calculated an average Chla fraction value for each phytoplankton group using the three sets of coefficients.

Simultaneously, *Tara* Oceans HPLC measurements (Pesant et al., 2015), which are available for the same stations and sampling time as for *psbO*, were considered to evaluate the correspondence between pigments and *psbO*-derived phytoplankton groups.
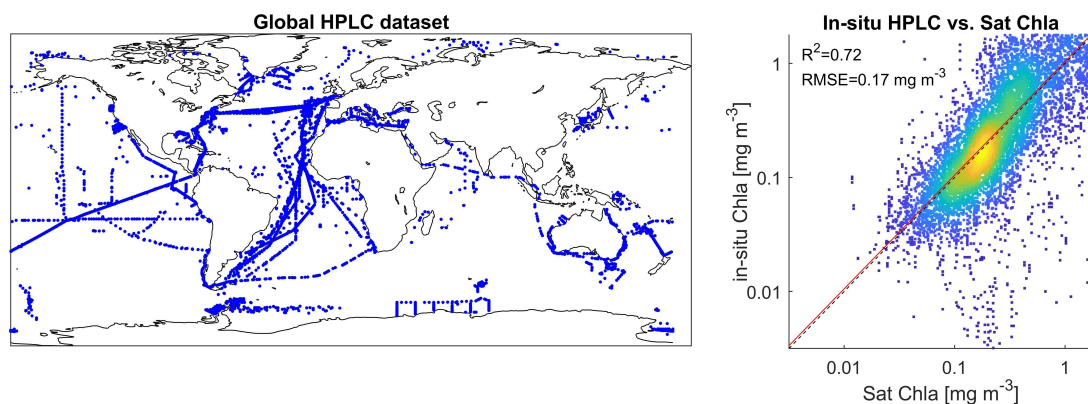

Figure 3. Geographical location of the global HPLC dataset stations regrouping observations from 1997 and 2014. The right panel represents a comparison between in-situ HPLC Chla measurement and its matchup using Globcolour Chla product.

2.3 PFT satellite products

In order to compare the outputs of our method to those of existing DPA-based remote sensing algorithms, we used two of them:

2.3.1 CMEMS phytoplankton Chla fraction

This Globcolour product contains the concentration of each phytoplankton functional type (expressed in terms of Chla concentration fraction) based on the Xi et al. (2020) algorithm, processed from 1997 to present. This algorithm estimates the Chla

Table 1. Phytoplankton groups and size classes associated with their diagnostic pigments and coefficients.

Phytoplankton size class	Phytoplankton group	Diagnostic Pigment (DP)	Coefficients (a)*		
			Uitz et al., 2006	Soppa et al., 2014	Brewin et al., 2015
Micro	**Diatoms**, Haptophytes, Chrysophytes, Dinoflagellates	Fucoxanthin (Fuco) (Jeffrey, 1980)	1.41	1.55	1.51
	Dinoflagellates	Peridinin (Perid) (Jeffrey, 1980; Jeffrey and Hallegraeff, 1987)	1.41	0.41	1.35
Nano	**Haptophytes**, Chrysophytes, Dinoflagellates	19'-Hexanoyloxyfucoxanthin (19HF) (Wright and Jeffrey, 1987)	1.27	0.86	0.95
	Green algae, Prasinophytes	Chlorophyll-b (Chlb) (Vidussi et al., 2001)	1.01	1.17	0.85
	Cryptophytes	Alloxanthin (Allo) (Gieskes and Kraay, 1983)	0.6	2.39	2.71
	Pelagophytes, Haptophytes	19'-Butanoyloxyfucoxanthin (19BF) (Wright and Jeffrey, 1987)	0.35	1.06	1.27
Pico	**Prokaryotes (Cyanobacteria)**, Green algae, Prasinophytes, Chrysophytes, Euglenophytes	Zeaxanthin (Dandonneau et al., 2004; Guillard et al., 1985)	0.86	2.04	0.93
Coefficients based on global HPLC dataset corresponding to the sum of the weighted diagnostic pigments to the total Chla; Chla=$\sum a$DP					

concentration of diatoms, dinoflagellates, haptophytes, green algae, and prokaryotes. The algorithm was implemented using

HPLC-based phytoplankton groups using the DPA approach (Soppa et al., 2014) and satellite reflectance in the visible spectrum (15 bands comprised between 400 and 709 nm) with empirical orthogonal function (EOF). This dataset is distributed by CMEMS (product number: OCEANCOLOUR_GLO_BGC_L3_MY_009_103).

2.3.2 SOM phytoplankton pigments

SOM-Pigments (El Hourany et al., 2019a) is a machine learning-based algorithm that allows the estimation of phytoplankton pigment concentrations in oceanic waters from satellite ocean color data (Chla, Rrs at four wavelengths: 412, 443, 490 and 555nm) and SST. This algorithm is based on the use of Self-Organizing Maps (SOMs), an unsupervised neural network, and was calibrated using the HPLC dataset described above.

The SOM-Pigments algorithm applied to Globcolour products allowed us to estimate the concentration of ten phytoplankton pigments (Chlorophyll-a (Chla), Divinyl-Chlorophyll-a (DVChla), Chlorophyll-b (Chlb), Divinyl-Chlorophyll-b (DVChlb), 19'Hexfucoxanthin (19HF), 19'Butfucoxanthin (19BF), Fucoxanthin (Fuco), Peridinin (Perid), Alloxanthin (Allo), Zeaxanthin (Zea)) at the global scale from 1997 to 2021. We then used the coefficients in Table 1 to convert pigments into the Chla concentration of five phytoplankton groups, namely diatoms, dinoflagellates, haptophytes, green algae and prokaryotes.

3 Methods

Several machine learning algorithms were used in this study. The algorithm to estimate phytoplankton groups from satellite data was built using SOM (Kohonen, 2013) and topology-constrained organization. This allowed us to confirm the non-linear relationships between phytoplankton group composition and satellite data through topology conservation. Next, we used the Ascending Hierarchical clustering algorithm to identify the large scale patterns generated by SOM. This allowed us to emphasize the predominant data structure learned by SOM and to characterize phytoplankton biomes. Finally, to characterize the differences between the DPA- and *psbO*-based approaches, we used Random Forest models to highlight the cumulative importance of a pigment composition to estimate a phytoplankton group abundance. In the following section, each methodology and algorithm are explained in detail.

3.1 Structure of the training and test databases

The initial dataset (D) consists of the 145 *Tara* Oceans observations of *psbO* relative abundance of the seven defined phytoplankton groups, the Chla fraction per group, and the associated matchups of 21 satellite-derived parameters (Chla, SST, Rrs at 15 wavelengths from 412 to 709nm, NFLH, Kd at 490m, PAR, and bbp at 443nm). The unclassified phytoplankton fraction was also considered, despite negligible values, to ensure coherence of the total phytoplankton pool. The matchups between satellite observations and in-situ observations were selected by considering 3x3 pixel boxes around the in-situ coordinates and +/- 1 day around the day of the in-situ measurement (El Hourany et al., 2019a, b). We built two sub-datasets, the first (D_{RCA}) relating *psbO*-derived relative cell abundance of the seven defined phytoplankton groups to the 17 satellite-derived parameters, and the

Table 2. Percentage of missing values within the initial database.

Tara Oceans	psbO		Sat							
D (145 stations)	Relative cell abundance	Chla fraction per group	Chla	Rrs 412-709 nm	SST	bbp443	Kd490	NFLH	PAR
Percentage of missing values	-	7%	18%	43-53%	30%	55%	53%	37%	14%

second (D_{ChlF}) joining *psbO*-derived Chla fraction per phytoplankton group and the same 17 satellite-derived parameters. We then constructed two algorithms, using either D_{RCA} or D_{ChlF}, both based on the same SOM methodology described below. Following the positioning of *Tara* Ocean's stations, and the distribution of Chla values within both datasets (Fig. A1), both algorithms are suitable for case 1 waters applications (i.e. open ocean).

All variables were normalized by their variance to homogenize weights. The rationale behind this is that the phytoplankton community should be treated as a whole; consequently, the variability of each phytoplankton group is dependent on each other in a relative way. D_{RCA} and D_{ChlF} both present missing values (Table 2), most likely due to cloud coverage or coastal/ice presence/proximity. In-situ *psbO*-based observations also contained missing values due to an absence of certain measurements at a given station. Since the in-situ dataset contains a low number of observations (145 stations), every observation is valuable. In order to overcome the several limitations faced with this training dataset, we used the SOM algorithm that can deal with missing values and allow a robust generalization in the case of limited observations (Jouini et al., 2013).

3.2 Self-Organizing map applied to *Tara* Oceans *psbO* data

3.2.1 General concept of SOM

The SOM algorithm is utilized for clustering multidimensional databases by assigning them to classes represented by a fixed network of neurons known as the SOM map. The SOM map consists of a rectangular grid of p x q neurons and defines a discrete distance between neurons, enabling the partitioning of the dataset. Each cluster is associated with a neuron and represented by a prototype vector. Observations in the dataset are assigned to the nearest neuron based on the Euclidean Norm. A key feature of SOM is its ability to provide topological ordering, where close neurons on the map correspond to similar observations in the data space. The estimation of a neuron's vector and the topological order is determined through a minimization process of a cost function that depends on the distance between the neuron and its assigned observation. SOMs have been widely employed to complete missing data, utilizing the truncated distance (TD) that considers only the existing components of the observation's vector, thus allowing for the integration of incomplete information.

3.2.2 Training phase

The implementation of the SOM methodology is summarized in Fig. 4 and 5. Briefly, we first split the *Tara* Oceans *psbO* datasets so as to obtain 80% of the data to train the SOM, and 20% of the data as a test set, the latter consisting of 30 observations with complete *psbO* information. We did this separately for D_{RCA} and D_{ChlF} sub-datasets so as to generate

SOMRCA, which stands for the algorithm specialized in relative cell abundance estimation, and SOMChlF for the algorithm specialized in Chla fraction per phytoplankton group.

During the SOM training, different combinations of satellite variables were used to determine the best set of variables to estimate the 7 phytoplankton groups in terms of relative cell abundance and Chla fraction. For each combination of variables, we increased the number of neurons from 10 to 1000 neurons to determine the optimal size of the SOM. For each SOM obtained, we quantified quantization and topographic errors. The quantization error represents the difference between an observation and its closest neuron. This error is monitored during the training procedure until it reaches stability at a minimum value with increasing training epochs. This is where the training should stop to prevent overfitting. The quantization error is expressed as follows:

$$qe = \frac{1}{n} \sum_{i=1}^{n} \|x_i - w_{ci}\|$$

where x_i is the vector of an input observation i; w_{ci} is the vector of the closest neuron c of a sample x_i; n is the number of observations.

However, the topographic error is a representation of having, for each observation of the database, distant first and second best-matching neurons and is expressed as follows:

$$te = \frac{1}{n} \sum_{i=1}^{n} d(x_i)$$

where $d(x_i) = 1$ if the first and second closest neuron to x_i are not adjacent, else $d(x_i)$=0.

Minimizing this quantity is important to ensure the preservation of the topological order within the SOM map with an increasing number of interpolated neurons. A one leave-out cross-validation procedure was performed to assign performance metrics (R^2 and RMSE) to help choose the best combination of SOM size and satellite variables. At each iteration of the cross-validation procedure, we chose randomly one observation as a test, whereas the other observations served to train the SOM with the given grid size. We calculated the closest neuron to the test observation based on its satellite variables only and associated these latter with the neuron's seven phytoplankton groups vector. When all the observations were used as a test, we calculated a mean R^2 and an RMSE, associated with the given size map, while comparing the estimated and observed phytoplankton group values. The best SOM configuration and variable combination are based on an optimum where te, qe, and the RMSE are in low ranges while avoiding overfitting. The chosen SOM was tested using the 20% test set, providing independent performance metrics to evaluate the generalization of the chosen SOM. As a result, we present in the paper the performance metrics of the chosen SOM configuration based on the cross-validation procedure and the test set.

The optimal combination of satellite parameters for the SOMRCA and SOMChlF algorithms was determined to be Chla, SST, Rrs at four wavelengths (412, 443, 490, and 555 nm), bbp, and Kd490. The grid size for SOMRCA was set at 242 neurons, while SOMChlF had a grid size of 222 neurons. This selection was based on several factors, including a high regression coefficient between estimated and observed phytoplankton values, low error values of quantization and topographic error, and

a low global RMSE encompassing all phytoplankton groups. The choice of Rrs bands aligns with previous work conducted on the PHYSAT method by Alvain et al. (2005) and Ben Mustapha et al. (2013). The PHYSAT method utilizes reflectance anomalies in the same four selected bands to identify dominant phytoplankton functional types. It should be noted that the Rrs

225   bands selected, including the additional 670 nm band, are commonly measured by all sensors used to build the Rrs product of Globcolour. This overlapping of different sensors enhances data availability and coverage, thus increasing the importance of these Rrs bands within the initial dataset. The inclusion of the Rrs at 670 nm did not significantly impact the performance of either SOMRCA or SOMChlF, primarily due to the open ocean nature of the dataset. In the clear open ocean, the information contained in the remote sensing reflectance (Rrs) bands beyond 555 nm is limited due to the strong absorption by water, as

230   noted by Xi et al. (2015).

Through the iterative training process described above, the results show a significant increase in the general performance of the method when the number of neurons increases to a certain extent (Fig. 6). Using a number of neurons larger than the training dataset still allows a refined discretization. In this case, some neurons will capture a sample of the database, which permits to define a referent vector for these neurons. When the neuron did not capture any data observation, the discrete distance between

235   the neighboring neurons was used to determine the referent vector w of each neuron that has not captured any data (Sarzeaud and Stephan, 2000; El Hourany et al., 2019a). This leads to preserving the topological order provided by new interpolated neurons. However, the quantization error's lowest values above 350 neurons might indicate overfitting.
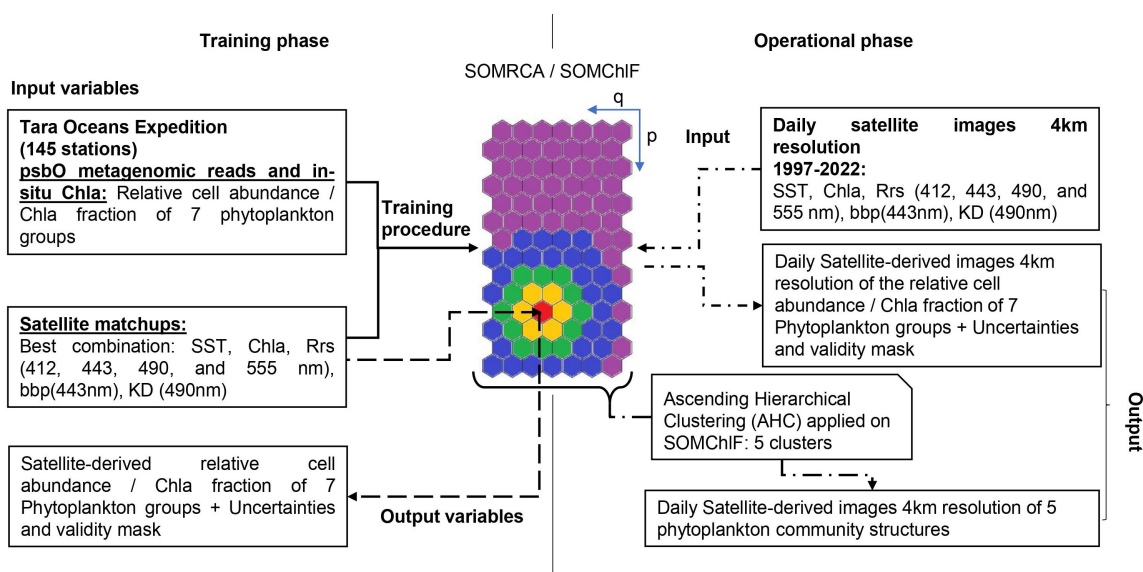

Figure 4. General flowchart of the SOM methodology applied on both D_{RCA} and D_{ChlF} to construct SOMRCA and SOMChlF.
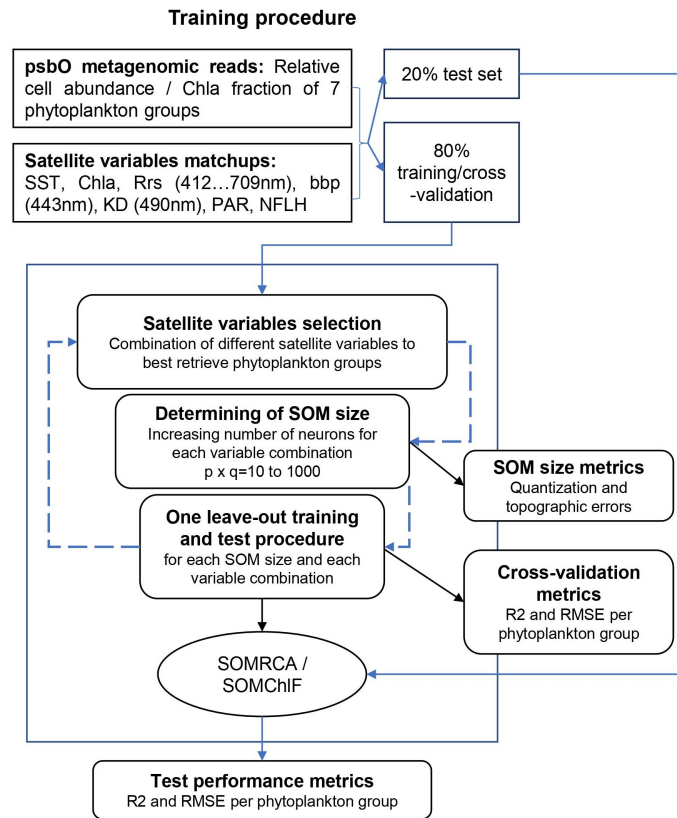
Training procedure

Figure 5. Detailed training procedure of the SOM methodology applied on both D_{RCA} and D_{ChlF}.

3.2.3 Operational phase

During the operational phase, we estimated the phytoplankton group variability using the best combination of satellite param-
eters. The set of parameters of a pixel was projected onto the SOM. In doing so, the parameters at each pixel were normalized
by the variance of that same parameter within the initial training dataset to maintain an equal weight among the parameters and
were assigned with the closest best-matching neuron using the truncated distance. At the end of the assignment phase, each
pixel was associated with a referent vector corresponding to the best matching neuron, which includes the seven phytoplankton
groups as a function of relative cell abundance in the case of SOMRCA, or Chla fraction in the case of SOMChlF. Since the
training was undergone for the whole phytoplankton community at once, alongside the total Chla information, the SOM allows
the inherent structure of the data to be preserved.

For this phase, level 3 mapped 4 km daily images were used to estimate the phytoplankton groups at the same spatio-temporal
resolution.
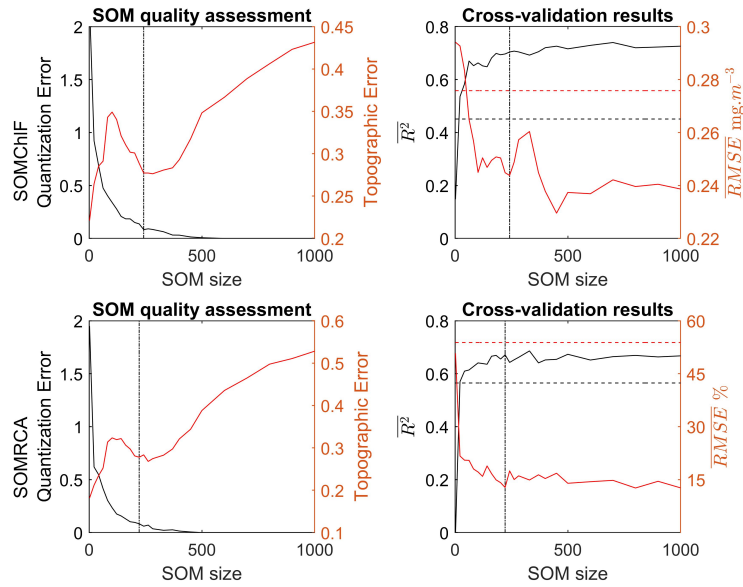
Figure 6. Quality assessment based on the quantization and topographic error related to the training of the SOMChlF and SOMRCA as a function of increasing SOM size (number of neurons) using Chla, SST, Rrs at 4 wavelengths (412, 443, 490 and 555 nm), bbp and Kd490. In parallel, the average regression coefficient and the root mean squared error as a function of increasing SOM size were calculated through a "one-leave out" cross-validation procedure. The dashed black and red lines correspond, respectively, to the R_2 and the RMSE using the "K-nearest neighbor" algorithm. Finally, the dotted lines correspond to the chosen SOM size for SOMChlF=242 neurons and SOMRCA=222 neurons.

3.2.4 Masking and uncertainty evaluation

250 Given that our initial dataset is of limited size, it is possible that it does not contain certain naturally occurring cases. In order to prevent abnormal predictions for cases not observed in the initial dataset, we conducted a quality evaluation of the method's output. This evaluation involved quantifying a reliability index by comparing the set of satellite parameters' values at a particular pixel with the values of the same parameters in the initial dataset. If a satellite variable's value fell outside the range defined within the initial dataset by the mean value of the same variable's distribution plus or minus two standard

255 deviations, it was considered distant. This evaluation was performed for all satellite variables per pixel, and the reliability index was determined by dividing the number of accepted variables by the total number of existing variables. A higher reliability index indicates greater reliability of the method, while regions with lower reliability index values require additional attention.

In the context of the global ocean, numerous uncertainties are associated with satellite parameters and regions. The SOM algorithm is known to effectively reduce noise and mitigate the impact of uncertainties within the dataset (da Silva and Costa,

260 2013). However, the main source of uncertainty in the estimation process stems from selecting the best matching neuron. This involves finding and associating the closest neuron in the SOM with a new or unfamiliar observation, such as a satellite pixel.

Due to the topology conservation, a pixel could be assigned to several close neurons, forming a neighborhood along a distance gradient. Consequently, a single satellite observation can represent various probabilities of phytoplankton group combinations.

To account for all uncertainties in the estimations, we opted to associate each pixel and phytoplankton group (based on relative cell abundance or Chla fraction) with a weighted standard deviation derived from the values of the ten closest neurons. The weights were determined by the distances between the first ten matching neurons and the pixel. This approach allowed us to incorporate uncertainties into the assignment process and provide a confidence measure for each pixel's assignment. By considering both the reliability index and the weighted standard deviation, we could assess the influence of uncertainties in the satellite variables.

3.3 Characterisation of phytoplankton biomes

To emphasize the predominant data structure learned by SOMChlF, the Ascending Hierarchical Clustering algorithm (AHC) was used to characterize phytoplankton biomes on the basis of their Chla fractions (a proxy of a phytoplankton group's biomass) and optical signature.

The HAC is a bottom-up clustering algorithm. The HAC starts with individuals and combines them according to their similarity (with respect to the chosen distance) to obtain new clusters. The exact number of biomes is not known a priori but at the end of the SOM+HAC procedure, several possibilities of a number of clusters to be taken into account were revealed. A compromise was made between the number of clusters we could explain from a physical point of view and the number of clusters for which we needed to include the maximum of information embedded in the dataset. This procedure has been used with success in several studies (Reygondeau et al., 2014; Richardson et al., 2003; Rossi et al., 2014; Sawadogo et al., 2009; El Hourany et al., 2021). At the end of the HAC clustering phase, each neuron of the SOMChlF was associated with a cluster. The association of several neurons in a cluster allows us to identify common phytoplankton community structures, and therefore characterize phytoplankton biomes. Upon applying SOMChlF as described in the operational phase section, each pixel of a satellite image could be associated with a cluster.

3.4 Evaluation of pigments to estimate phytoplankton groups

Each phytoplankton group's *psbO* abundance was associated with its corresponding HPLC pigments measurement performed on the same *Tara* Oceans station. The ability of pigments to predict phytoplankton groups was evaluated using a bagged random forest algorithm (number of learners set to 200), following the permutation-based importance method.

The bagged random forest algorithm is a set of decision trees, each constituted of internal nodes and leaves. In the internal node, the selected feature (i.e., pigment in this case) was used to make a decision on how to divide the dataset into separate sets with similar responses in terms of a given phytoplankton group. Since this algorithm is used in a case of regression, the decision is evaluated while monitoring the error decrease between the real phytoplankton group abundance and the predicted one, which corresponds to the value of a divided set. The permutation-based importance method will randomly shuffle each pigment and compute the change in the model's performance to predict the abundance of a phytoplankton group.

Table 3. Results of the cross-validation and test exercises of SOMRCA and SOMChlF based on the regression coefficient (R^2) and the root-mean-squared-error (RMSE).

Phytoplankton group	SOMRCA Relative cell abundance (%)				SOMChlF Phytoplankton chlorophyll-a fraction (mg m-3)			
	Cross-val		Test		Cross-val		Test	
	R^2	RMSE (%)	R^2	RMSE (%)	R^2	RMSE ($mg.m^{-3}$)	R^2	RMSE ($mg.m^{-3}$)
Diatoms	0.65	2.70	0.72	2.00	0.66	0.25	0.86	0.04
Dinoflagellates	0.79	5.45	0.83	6.15	0.65	0.09	0.61	0.04
Green Algae	0.61	5.64	0.67	4.32	0.71	0.03	0.62	0.01
Haptophytes	0.66	3.42	0.33	3.04	0.76	0.07	0.68	0.01
Prokaryotes	0.60	19.27	0.67	20.53	0.57	0.05	0.76	0.09
Cryptophytes	0.62	1.98	0.78	1.98	0.70	0.03	0.77	0.01
Pelagophytes	0.64	2.60	0.36	1.96	0.68	0.02	0.74	0.01
Chlorophyll-a					0.83	0.23	0.72	0.31

Using this method, a pigment composition of the seven major phytoplankton pigments cited in Table 1 was tested to predict the abundance of each *psbO*-derived phytoplankton group, and therefore estimate their importance. The concentration of each pigment was evaluated in terms of pigment ratios, a ratio relative to the sum of all pigments' concentration, and in parallel, the *psbO*-derived relative abundance was used.

4 Results and discussion

4.1 Cross-validation, performances, and spatial limitation of the SOMRCA and SOMChlF algorithms

Cross-validation of different combinations of satellite data and SOM grid size revealed a performance of an average R^2 of 0.68 for SOMRCA and of 0.74 for SOMChlF (Fig. 7, table 3). Upon summing all Chla fractions, the cross-validation analysis shows a satisfying agreement between estimated total Chla and in-situ values ($R^2 = 0.83$) and therefore a preservation of the initial phytoplankton quantity expressed in total Chla.

To evaluate the quality of the representation of the inter-variable relationships within the input data by the SOM, the correlation coefficients and phytoplankton group value distributions were compared between the vectors constituting the neurons of SOMRCA and SOMChlF with D_{RCA} and D_{ChlF}, respectively. This analysis showed that the correlation coefficients were not altered within SOMRCA nor SOMChlF, and neither was the shape of the distribution of the values while compared to the initial dataset. These results highlight the capacity of SOM to preserve the characteristics of the initial dataset after the training procedure (Fig. A1 and A2).
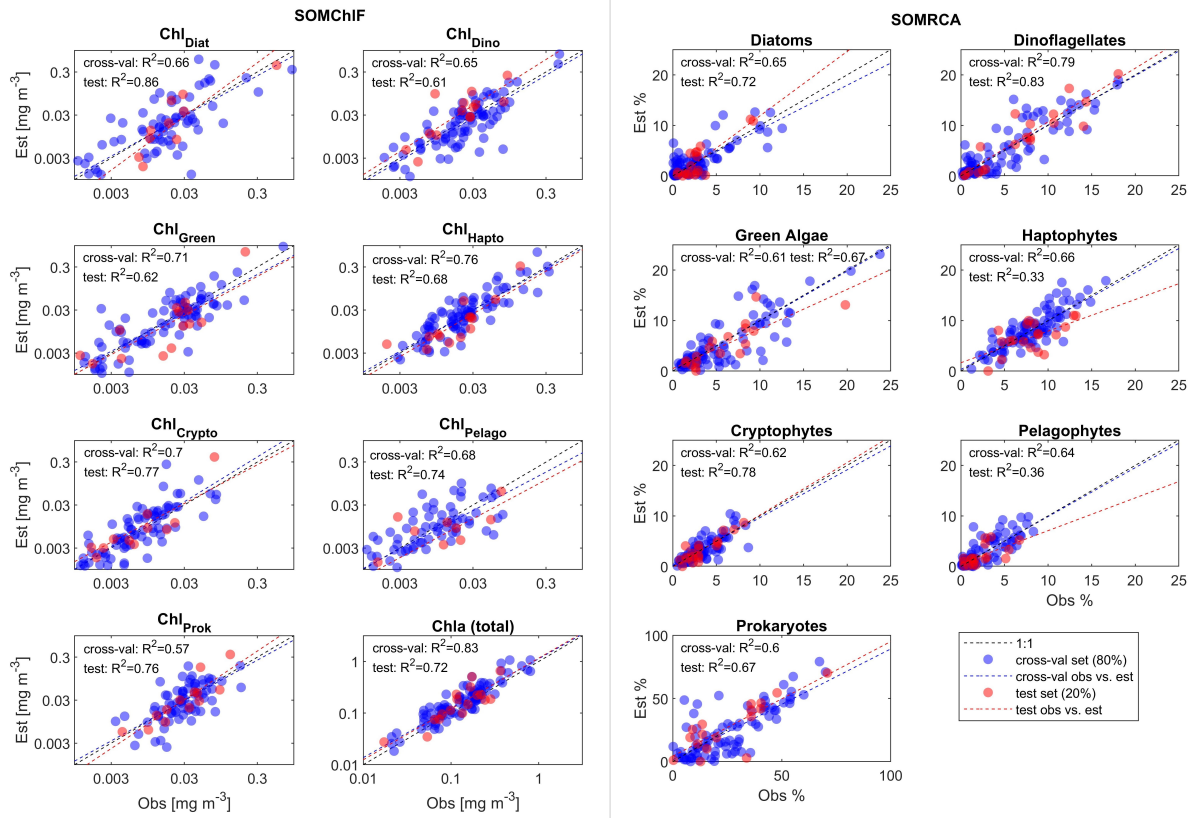
Figure 7. Results of the two-step cross-validation (blue) and test (red) procedures for SOMChlF (left) and SOMRCA (right) with the chosen best combination of satellite parameters and a SOM grid, respectively, of 242 and 222 neurons. For the cross-validation, each observation, among 80% of the initial data, was used iteratively as a training set and as a test set until all observations served as tests (blue dots). This procedure was used to identify the best satellite combination and SOM grid size. Finally, the remaining 20% was used as a test to evaluate the generalization capacity of the SOM with the chosen configuration (red dots).

310   However, given the limited size of the initial dataset, applying SOMRCA and SOMChlF to the global satellite data must be done with caution. For each pixel and at each time step between 1997 to 2021, we performed the quality control described in section 3.2.3 to provide a measure of the applicability of this method (Fig. 8). Regions of low confidence can be identified where the value of the reliability index does not exceed 40% throughout the time series. These regions are mainly found in coastal and turbid waters, as well as the South Pacific Ocean gyre, and are characterized either by very high or very low Chla

315   values. This result is expected because the SOM algorithm is mainly adapted for case 1 waters and cannot extrapolate beyond the distribution of values in the initial dataset. Furthermore, moderate confidence regions in which around 20% of the pixels fall out of the accepted bounds, are highlighted by a reliability index under 80%. These regions are mainly found at high latitudes, especially in the Southern Ocean, mainly due to the limited number of available samples in the area and the particular optical characteristics of that region (Mitchell et al., 1991).

320   Uncertainty values reached 20% relative cell abundance for SOMRCA and 0.15 $mg.m^{-3}$ of Chla SOMChlF, respectively, and in each case displayed regional patterns. Generally, uncertainty values followed the concentration gradient in Chla fraction and cell abundance per group. High latitudes exhibited the highest uncertainties for diatoms, green algae, and haptophyte relative cell abundances, while the Southern Ocean showed the highest uncertainties for prokaryotic cell abundance. The elevated uncertainty in prokaryotes within the Southern Ocean can be attributed to the limited sampling in this area, resulting

325 in greater dissimilarity between satellite data in this region and the data sampled in the initial dataset, corroborating the findings of the reliability index. This is also consistent with the very low abundance of cyanobacteria in the area (Flombaum et al., 2013), for which model uncertainty may be higher.
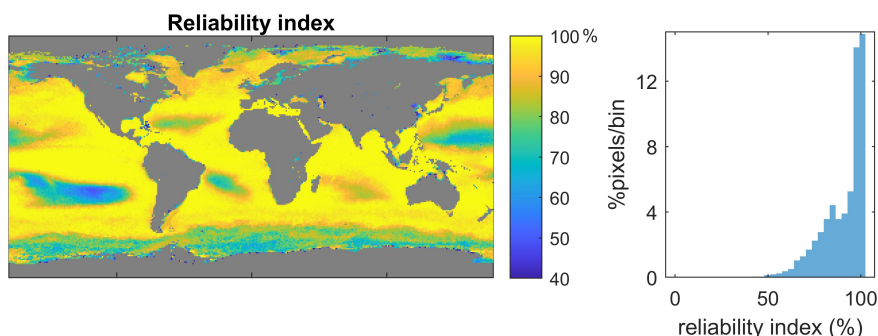
Figure 8. Applicability of the satellite *psbO*-based method. The geographical (left) and values distribution (right) of the reliability index were calculated between 1997 and 2021 by testing the set of satellite parameters at a given pixel against the values in the original dataset (D).

4.2   Comparison with global HPLC pigment dataset

       The global in-situ HPLC dataset was then used to estimate Chla fractions for each phytoplankton group using the diagnos-

330 tic pigment approach (DPA). This dataset was compared to the Chla fraction matching each phytoplankton group that was estimated by SOMChlF (Fig. 9). Evaluating the sum of Chla fractions and comparing it with in-situ Chla can be considered as a baseline evaluation of this method. This comparison showed a satisfying correspondence score of R^2=0.72. Relatively good correspondence is noted for diatoms and haptophytes, showing an R^2=0.64 between in-situ and SOMChlF for diatoms and 0.65 for haptophytes. Moderate correspondence was found for green algae, cryptophytes, and pelagophytes, with an R^2

335 ranging between 0.43 and 0.39. Prokaryotes and dinoflagellates had the lowest correspondence between both outputs. The comparison between DPA-based phytoplankton groups and SOMChlF estimates is highly uncertain. It compares two types of information indicating the same phytoplankton group, with different underlying assumptions about how to define and describe a certain group. For some of the groups, these results are coherent. For example, the diatom Chla fraction is well captured by the latter, and the values agree with those estimated using HPLC observations; however, we noted a major overestimation

340 within the HPLC DPA method. For prokaryotes, this comparison leads us to say that the use of zeaxanthin as an indicator of the cyanobacterial contribution to Chla may not be entirely representative of this group.

17

The permutation-based importance analysis using Random Forest, performed on the in-situ *Tara* Oceans *psbO* and HPLC measurements, emphasizes the necessity of a multivariate approach for predicting phytoplankton community structure based on pigments (see Fig. 10). Notably, the diagnostic pigments mentioned in Table 1 exhibited dominant importance in determining the relative abundance of their respective assigned phytoplankton groups. For instance, peridinin represented dinoflagellates, Chlorophyll-b characterized green algae, and zeaxanthin indicated prokaryotes (Table 1). These pigments demonstrated the highest importance for their respective groups, as illustrated in Fig. 10, accompanied by a positive Spearman correlation. However, individually, these pigments accounted for less than 25% of the variance in their respective groups. Conversely, in the case of cryptophytes, diatoms, and haptophytes, no pigment stood out in terms of importance, and the observed correlations were related to co-variation between pigments (e.g., Chlb and Fuco in diatoms), possibly influenced by Chla variability. Therefore, the variability within each group is best explained not by a single diagnostic pigment, but rather by the overall pigment composition. It is crucial to consider how natural variability can influence the interpretation of pigment composition in relation to phytoplankton community structure. Pigment ratios not only vary with phytoplankton composition but also reflect the diverse strategies employed by different phytoplankton types to acclimate to environmental factors such as light, temperature, nutrients, and other variables.

4.3 Global patterns of satellite-derived phytoplankton groups

We then applied our method to Glocolour satellite data to generate a daily database spanning from 1997 to 2021, capturing the relative cell abundance and Chla fraction of seven phytoplankton groups of interest. Fig. 101 presents the annual patterns of relative cell abundance and Chla fraction for each phytoplankton group, derived from this satellite dataset.

Regarding relative cell abundance, the prokaryotes stand out as a dominant group. This group largely dominated tropical regions, with a relative abundance of up to 80% in subtropical gyres. Haptophytes, green algae, and diatoms exhibited higher abundance in mid and high latitudes as well as the equatorial region, showing a maximum relative abundance of 30%. The remaining three phytoplankton groups displayed relative abundances that barely exceeded 10% of the total phytoplankton community. Pelagophytes and dinoflagellates were primarily observed in mid and subtropical latitudes, while cryptophytes were found in coastal areas and high latitudes.

Examination of how each phytoplankton group contributed to total Chla revealed that diatoms had a significant contribution at high latitudes and equatorial regions. Prokaryotes, on the other hand, had an overall low to moderate contribution to total Chla.

Qualitatively, the information captured by SOMChlF was clustered into five groups, each characterized by a distinct remote sensing reflectance spectrum that corresponded to the phytoplankton community structure (Fig. 112). To illustrate the link between each group's contribution to total Chla concentration and relative cell abundance, we depicted the latter while evaluating the pixel's assigned relative abundance values for each of the five clusters. This approach revealed that three out of the five clusters are dominated by prokaryotes in terms of cell abundance (C1, C2, and C3). However, based on their relative contribution to Chla, C1 was found to be dominated by prokaryotes and dinoflagellates, C2 exhibited a mixed composition, C3, and C4
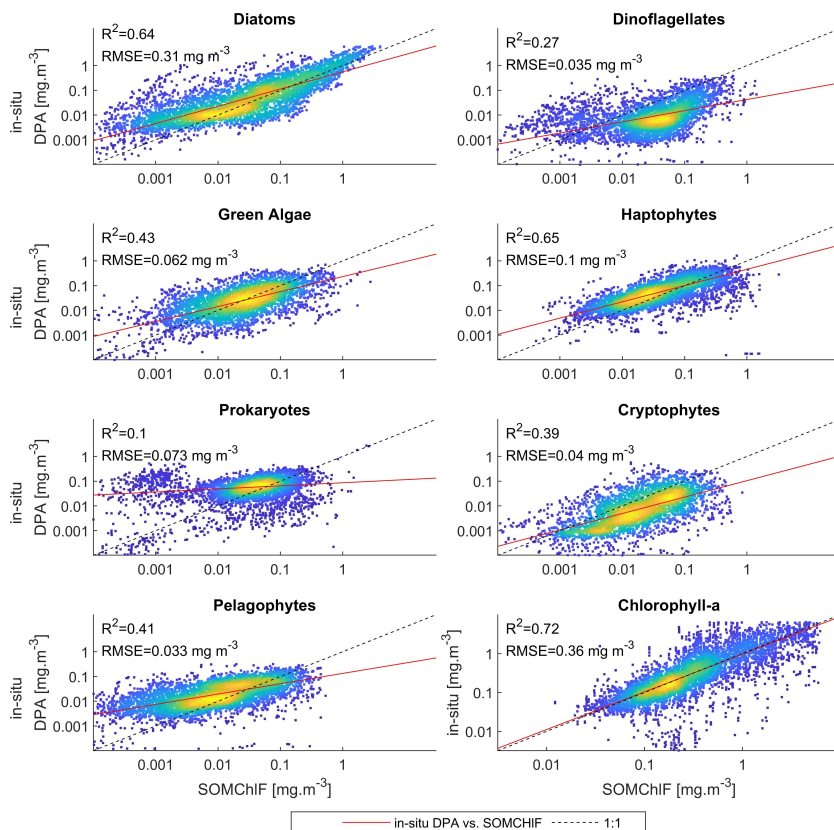
Figure 9. Comparison between the outputs of SOMChlF and the DPA approach applied on an in-situ global HPLC dataset.

represented diatoms and other eukaryotes, whereas C5 was predominantly composed of diatoms. The shift from relative cell abundance to size-integrated relative Chla fraction illustrates how cell size influences Chla contribution and variability.

Each cluster is characterized by a specific optical signature in terms of Rrs spectra. The Rrs values per wavelength were normalized based on their corresponding variance, enabling intercomparison regardless of magnitude. For instance, C1, which exhibits higher reflectance in the blue wavelength, represents clear, oligotrophic waters. In such environments with low nutrients and high surface stratification, picophytoplankton groups like cyanobacteria thrive due to their high surface-to-size ratio (Raven, 1998; Chisholm, 1992). C2 represents normalized Rrs spectra with insignificant differences between normalized bands, suggesting an average state where the phytoplankton community appears mixed. In C3 and C4, we observed an increase in normalized Rrs values in the green compared to the blue wavebands, indicating higher Chla in these environments. Given that C3 and C4 are located in high-latitude regions with ample nutrient resources and exceptional seasonal variability of light intensity, larger cell-sized phytoplankton groups, including diatoms, are favored, leading to increased biomass and Chla con-

19
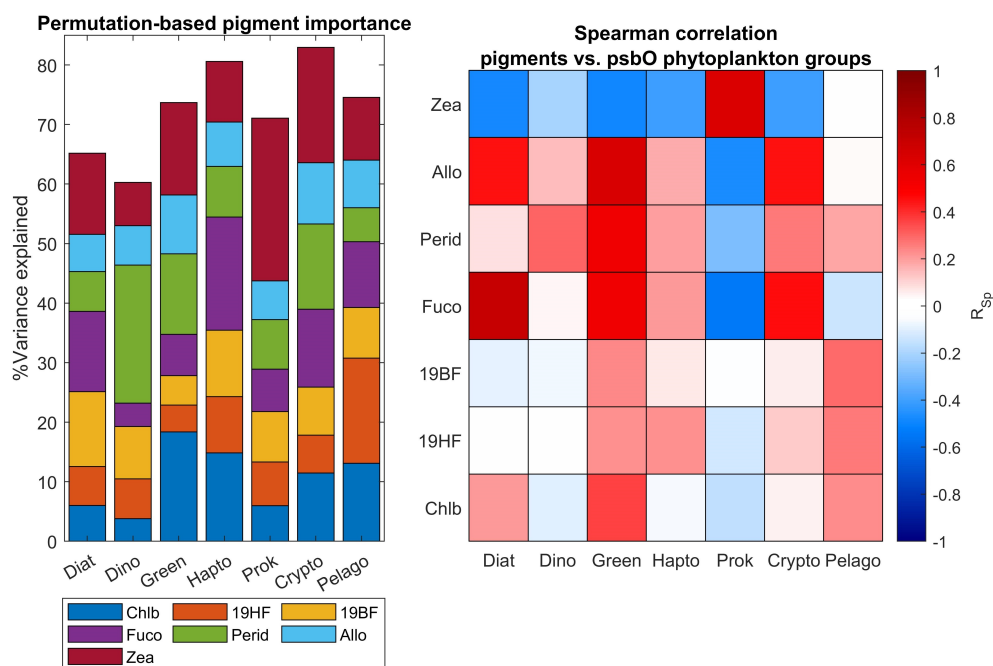
Figure 10. Evaluation of secondary pigment weighting for the estimation of different phytoplankton groups. The left panel represents the percentage of variance of each phytoplankton group explained by a set of frequently used phytoplankton secondary pigments. This analysis has been done using a random forest algorithm applied to the in-situ *Tara* Oceans *psbO* and HPLC datasets. A Spearman correlation coefficient has been calculated between each pigment and the phytoplankton groups (right panel).

tribution (Brun et al., 2015). C5, with the greatest difference between Rrs in the blue and green, represents eutrophic waters, known for their high productivity and diatom-dominated blooms (Brun et al., 2015).

Based on the global distributions of these clusters, several biomes can be defined. C1 is centered in subtropical gyres, C2 is found in transitional zones such as mid-latitude regions and the equatorial region, C3 is observed in the Southern Ocean, C4 corresponds to high-latitude regions, and C5 is prevalent in coastal and eutrophic waters.

Different temporal variability is evident for each cluster across different latitudinal bands. In northern high latitudes, an increase in C5 indicates maximal productivity occurring in that region around May. At mid-latitudes, the winter maximum is marked by an increase in C5 and C4 clusters. A secondary, less pronounced peak can be observed in autumn, attributed to the break in the thermocline and remineralization processes. During summer, C1 dominates the mid-latitude regions. In tropical regions, C1 is predominant, with a cyclic increase of C2 suggesting coastal influences, likely due to the proximity of C2 to nutrient-rich zones like upwelling systems. In contrast to northern high latitudes, the Southern Ocean exhibits a different temporal variability. The presence of prokaryotes is signified by C1 in this region, whereas C3 dominates during the bloom

season in January. This analysis confirms the Antarctic nature of C3 in contrast to C4, highlighting differences in water types between the two regions based on phytoplankton community structure and satellite data.

400 This division into parallel and transitional biomes underscores the significant influence of latitudinal physical gradients, including light availability and temperature, on the structuring of the phytoplankton community in terms of types and size. These findings align with previous global phytoplankton studies conducted in situ (Ibarbalz et al., 2019; Sommeria-Klein et al., 2021) as well as satellite estimates (Alvain et al., 2006; Hirata et al., 2011; Ben Mustapha et al., 2013; El Hourany et al., 2019a; Xi et al., 2020).

405 **4.4 Intercomparison of satellite-derived phytoplankton group products**

A comparison was performed between SOMChlF's output, and two operational products based on Xi et al., 2020 and SOM-Pigments (El Hourany et al., 2019a) algorithms. We based this on the five phytoplankton groups common to all three algorithms: diatoms, dinoflagellates, green algae, haptophytes, and prokaryotes. The annual patterns show a substantial agreement between all three satellite-derived phytoplankton estimates (Fig. 13). However, some differences between the estimated quantities of
410 Chla phytoplankton groups can be noted. For diatoms, the outputs based on El Hourany et al. (2019a) and SOMChlF exhibit higher Chla values, while those based on Xi et al. (2020) show low values near the equatorial latitudes. For green algae and haptophytes, the three products show matching latitudinal variability, with only minor discrepancies in values at high and subtropical latitudes. For prokaryotes, the outputs of Xi et al. (2020) show higher estimates, particularly near the Arctic and equatorial regions. Lastly, for dinoflagellates, the SOM-Pigments method yielded lower Chla values, especially in subtropical
415 gyres, whereas SOMChlF showed the highest Chla estimates for this taxonomic group.

Addressing the differences between the outputs referring to the same phytoplankton group is not a straightforward task. Two methods are based on the DPA approach, which displays uncertainties related to the choice of pigments to delimit certain groups. For instance, several studies showed that the DPA approach tends to overestimate diatoms Brewin et al. (2014); Chase et al. (2020). This approach may compromise the relevance of satellite images when used. However, the added value of such an
420 approach resides in the availability of the large HPLC dataset, which allows the development of robust algorithms. On the other hand, the method described in this paper and the generated outputs are based for the first time on a complete and harmonized database of phytoplankton taxonomic community structure on a global scale; an approach that provides an unbiased picture of phytoplankton cell abundances. However, the major limitation of this approach at this time is the low number of observations from which the metric has been derived.

425 **5 Conclusions**

By employing an alternative approach utilizing in-situ metagenomic observations, a reliable ocean color algorithm for detecting phytoplankton groups was developed in this work. This achievement is noteworthy considering the limited availability of omics data used in our analysis. The successful implementation was made possible by leveraging machine learning techniques and preserving the data structure using Self-Organizing Maps. The methodology demonstrated satisfactory performance in
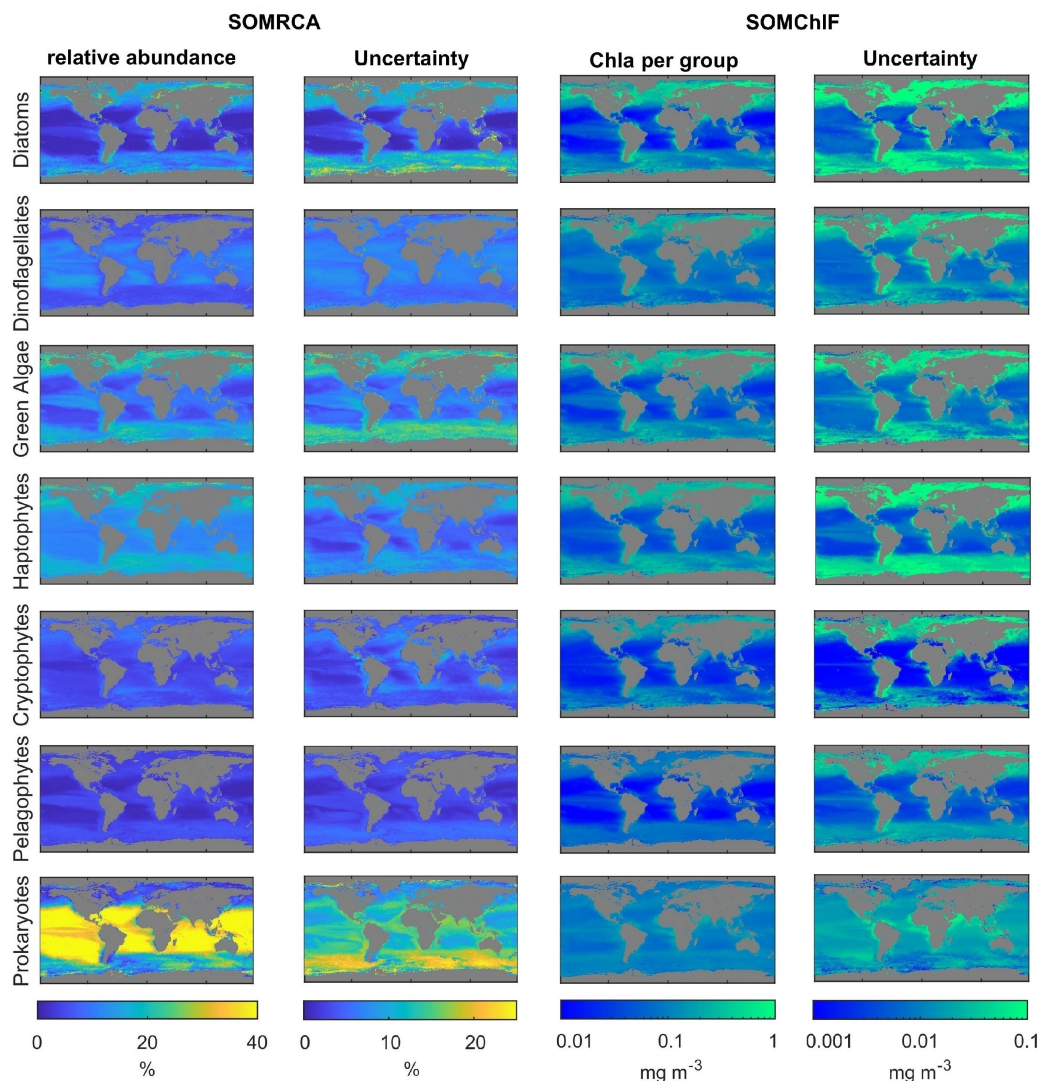
Figure 11. Annual composites of the relative abundances and Chl fractions of the seven *psbO*-derived phytoplankton groups based on satellite data (compiled using data from 1997-2021). The uncertainties related to each group and each method are because of their different possible combinations through the weighted standard deviations, as described in Section 3.2.3. We note that the scales for uncertainty are smaller than those in the abundance and Chla columns.

430 producing robust estimates for the seven major phytoplankton groups, albeit with some limitations in terms of global generalization due to the limited availability of data. For instance, it is important to exercise caution when interpreting estimates for regions such as the subtropical gyres. As DNA sequencing costs continue to decrease and new expeditions generate molecular data from undersampled ocean regions, we expect the training datasets to increase rapidly in future years, which should further
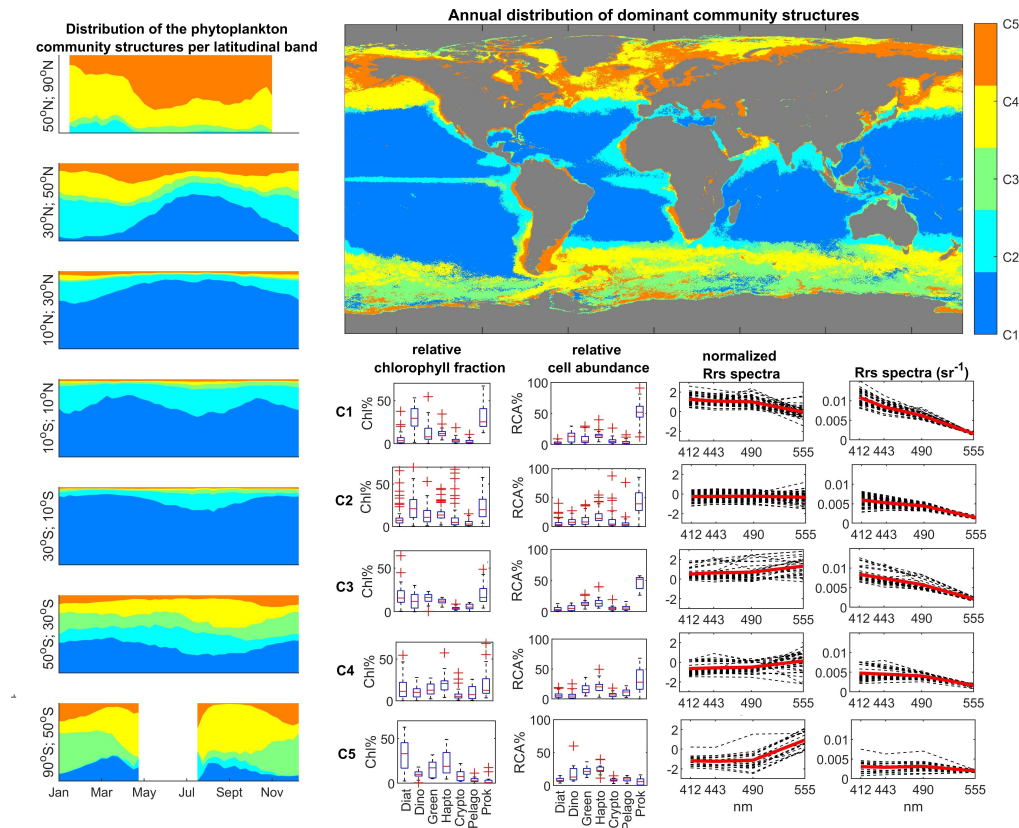
Figure 12. Satellite-derived biomes of phytoplankton communities, obtained by unsupervised clustering (Hierarchical clustering) of SOM-ChlF neurons. Normalized relative cell abundances and original Rrs spectra were also derived. The global map shows the most frequent community structure recorded during the 1997-2021 period. A spatio-temporal analysis was conducted to highlight latitudinal patterns.

increase the accuracy of our method. Furthermore, this study presents a new global dataset of the relative cell abundances of
the seven phytoplankton groups and their contributions to total Chla. These two types of information carry different implications. Chla serves as a biomass proxy, which is crucial for energy and matter fluxes in various ecological and biogeochemical processes. On the other hand, cell abundance represents species abundance for unicellular organisms, providing insights into community assembly processes.

This dataset opens up possibilities for inter-comparisons with existing approaches, such as DPA-based methods using in-situ and satellite data. The results provide coherent yet distinct information about phytoplankton communities, contributing to a better understanding of their composition. While our focus was on seven broad phytoplankton groups, it is worth mentioning that the deep taxonomic resolution achievable through molecular methods allows for species-level monitoring, which can be an interesting avenue for future implementation.
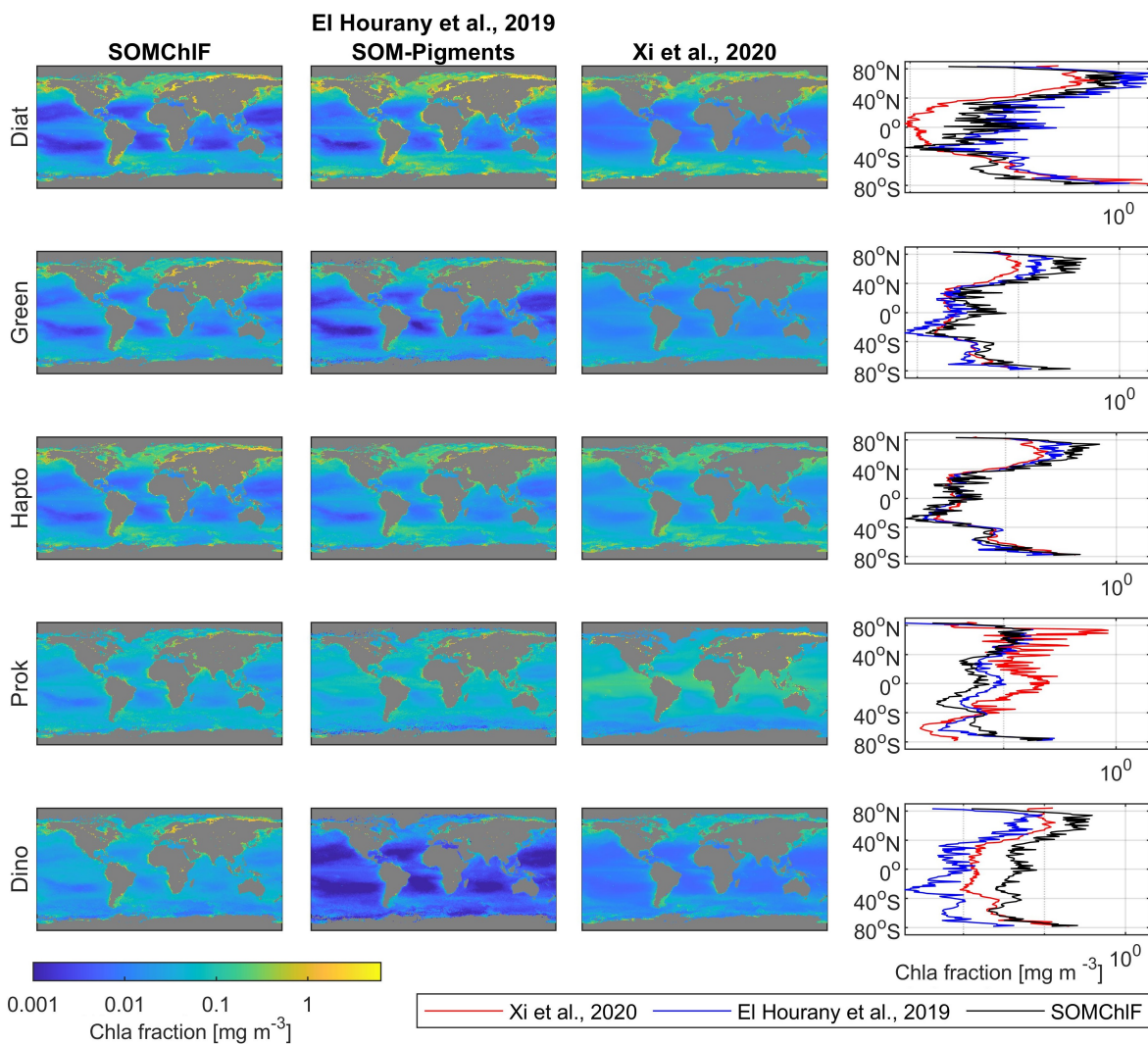
Figure 13. intercomparison of five satellite-derived phytoplankton group Chla fractions based on SOMChlF, SOM-Pigments (El Hourany et al., 2019a), and Xi et al. (2020) algorithms. The average per latitude of each Chla fraction is calculated to reveal latitudinal patterns (right panels).

The methodology presented in this work provides a unique opportunity to observe in real-time and high-resolution the state of the major phytoplankton groups at the global scale. This makes remote sensing observations excellent tools to collect EBVs, play the role of broker between monitoring initiatives and decision-makers, and provide a foundation for developing marine biodiversity forecasts under different policy and management scenarios. To reach this objective, remote sensing data inherently needs to be validated with in-situ observations as well. Of further interest is the impending PACE mission launch, a strategic climate continuity mission that will make global hyperspectral ocean color measurements possible. This will allow extended

450 data records on ocean ecology and global biogeochemistry, revolutionizing the detection of phytoplankton communities from space. From the perspective of PACE, this study is a step towards further understanding the effect of environmental changes on phytoplankton community structure and diversity.

References

Aiken, J., Pradhan, Y., Barlow, R., Lavender, S., Poulton, A., Holligan, P., and Hardman-Mountford, N.: Phytoplankton pigments and functional types in the Atlantic Ocean: A decadal assessment, 1995-2005, Deep-Sea Research Part II: Topical Studies in Oceanography, 56, 899–917, https://doi.org/10.1016/j.dsr2.2008.09.017, 2009.

480

Alvain, S., Moulin, C., Dandonneau, Y., and Bréon, F.: Remote sensing of phytoplankton groups in case 1 waters from global SeaWiFS imagery, Deep Sea Research Part I: Oceanographic Research Papers, 52, 1989–2004, https://doi.org/10.1016/j.dsr.2005.06.015, 2005.

Alvain, S., Moulin, C., Dandonneau, Y., Loisel, H., and Bréon, F. M.: A species-dependent bio-optical model of case I waters for global ocean color processing, Deep-Sea Research Part I: Oceanographic Research Papers, 53, 917–925, https://doi.org/10.1016/j.dsr.2006.01.011, 2006.

485

Alvain, S., Moulin, C., Dandonneau, Y., and Loisel, H.: Seasonal distribution and succession of dominant phytoplankton groups in the global ocean: A satellite view, Global Biogeochemical Cycles, 22, 1–15, https://doi.org/10.1029/2007GB003154, 2008.

Ben Mustapha, Z., Alvain, S., Jamet, C., Loisel, H., and Dessailly, D.: Automatic classification of water-leaving radiance anomalies from global SeaWiFS imagery: Application to the detection of phytoplankton groups in open ocean waters, Remote Sensing of Environment, https://doi.org/10.1016/j.rse.2013.08.046, 2013.

490

Bracher, A., Vountas, M., Dinter, T., Burrows, J. P., Röttgers, R., and Peeken, I.: Quantitative observation of cyanobacteria and diatoms from space using PhytoDOAS on SCIAMACHY data, Tech. rep., www.biogeosciences.net/6/751/2009/, 2009.

Bracher, A., Taylor, M. H., Taylor, B., Dinter, T., R??ttgers, R., and Steinmetz, F.: Using empirical orthogonal functions derived from remote-sensing reflectance for the prediction of phytoplankton pigment concentrations, Ocean Science, 11, 139–158, https://doi.org/10.5194/os-11-139-2015, 2015.

495

Brewin, R. J., Sathyendranath, S., Jackson, T., Barlow, R., Brotas, V., Airs, R., and Lamont, T.: Influence of light in the mixed-layer on the parameters of a three-component model of phytoplankton size class, Remote Sensing of Environment, 168, 437–450, https://doi.org/10.1016/J.RSE.2015.07.004, 2015.

Brewin, R. J. W., Sathyendranath, S., Tilstone, G., Lange, P. K., and Platt, T.: A multicomponent model of phytoplankton size structure, Journal of Geophysical Research: Oceans, 119, 3478–3496, https://doi.org/10.1002/2014JC009859, 2014.

500

Brown, C.: Global Distribution of Coccolithophore Blooms, Oceanography, 8, 59–60, https://doi.org/10.5670/oceanog.1995.21, 1995.

Brun, P., Vogt, M., Payne, M. R., Gruber, N., O'brien, C. J., Buitenhuis, E. T., Le Quéré, C., Leblanc, K., and Luo, Y.-W.: Ecological niches of open ocean phytoplankton taxa, Limnology and Oceanography, 60, 1020–1038, 2015.

Chase, A. P., Kramer, S. J., Haëntjens, N., Boss, E. S., Karp-Boss, L., Edmondson, M., and Graff, J. R.: Evaluation of diagnostic pigments to estimate phytoplankton size classes, Limnology and Oceanography: Methods, 18, 570–584, https://doi.org/10.1002/LOM3.10385, 2020.

505

Chisholm, S. W.: Phytoplankton size, Primary productivity and biogeochemical cycles in the sea, pp. 213–237, 1992.

da Silva, L. E. B. and Costa, J. A. F.: Clustering, noise reduction and visualization using features extracted from the self-organizing map, in: Intelligent Data Engineering and Automated Learning–IDEAL 2013: 14th International Conference, IDEAL 2013, Hefei, China, October 20-23, 2013. Proceedings 14, pp. 242–251, Springer, 2013.

510

Dandonneau, Y., Deschamps, P.-Y., Nicolas, J.-M., Loisel, H., Blanchot, J., Montel, Y., Thieuleux, F., and Bécu, G.: Seasonal and interannual variability of ocean color and composition of phytoplankton communities in the North Atlantic, equatorial Pacific and South Pacific, Deep Sea Research Part II: Topical Studies in Oceanography, 51, 303–318, https://doi.org/10.1016/j.dsr2.2003.07.018, 2004.

de Salas, M. F., Eriksen, R., Davidson, A. T., and Wright, S. W.: Protistan communities in the Australian sector of the Sub-Antarctic Zone during SAZ-Sense, Deep Sea Research Part II: Topical Studies in Oceanography, 58, 2135–2149, 2011.

515 Di Cicco, A., Sammartino, M., Marullo, S., and Santoleri, R.: Regional Empirical Algorithms for an Improved Identification of Phytoplankton Functional Types and Size Classes in the Mediterranean Sea Using Satellite Data, Frontiers in Marine Science, 4, 126, https://doi.org/10.3389/fmars.2017.00126, 2017.

Dutkiewicz, S., Cermeno, P., Jahn, O., Follows, M. J., Hickman, A. A., Taniguchi, D. A., and Ward, B. A.: Dimensions of marine phytoplankton diversity, Biogeosciences, 17, 609–634, https://doi.org/10.5194/BG-17-609-2020, 2020.

520 El Hourany, R., Abboud-Abi Saab, M., Faour, G., Aumont, O., Crépon, M., and Thiria, S.: Estimation of secondary phytoplankton pigments from satellite observations using self-organizing maps (SOM), Journal of Geophysical Research: Oceans, https://doi.org/10.1029/2018JC014450, 2019a.

El Hourany, R., Abboud-Abi Saab, M., Faour, G., Mejia, C., Crépon, M., and Thiria, S.: Phytoplankton Diversity in the Mediterranean Sea From Satellite Data Using Self-Organizing Maps, Journal of Geophysical Research: Oceans, 124, 5827–5843, 525 https://doi.org/10.1029/2019JC015131, 2019b.

El Hourany, R., Mejia, C., Faour, G., Crépon, M., and Thiria, S.: Evidencing the Impact of Climate Change on the Phytoplankton Community of the Mediterranean Sea Through a Bioregionalization Approach, Journal of Geophysical Research: Oceans, 126, e2020JC016 808, https://doi.org/10.1029/2020JC016808, 2021.

Flombaum, P., Gallegos, J. L., Gordillo, R. A., Rincon, J., Zabala, L. L., Jiao, N., Karl, D. M., Li, W. K. W., Lomas, M. W., Veneziano, D., 530 Vera, C. S., Vrugt, J. A., and Martiny, A. C.: Present and future global distributions of the marine Cyanobacteria Prochlorococcus and Synechococcus, Proceedings of the National Academy of Sciences, 110, 9824–9829, https://doi.org/10.1073/pnas.1307701110, 2013.

Fragoso, G. M., Poulton, A. J., Yashayaev, I. M., Head, E. J. H., and Purdie, D. A.: Spring phytoplankton communities of the Labrador Sea (2005-2014): pigment signatures, photophysiology and elemental ratios, Biogeosciences Discussions, pp. 1–43, https://doi.org/10.5194/bg-2016-295, 2016.

535 Fuhrman, J. A.: Microbial community structure and its functional implications, https://doi.org/10.1038/nature08058, 2009.

Guidi, L., Stemmann, L., Jackson, G. A., Ibanez, F., Claustre, H., Legendre, L., Picheral, M., and Gorsky, G.: Effects of phytoplankton community on production, size, and export of large aggregates: A world-ocean analysis, Limnology and Oceanography, 54, 1951–1963, https://doi.org/10.4319/LO.2009.54.6.1951, 2009.

Henson, S. A., Cael, B. B., Allen, S. R., and Dutkiewicz, S.: Future phytoplankton diversity in a changing climate, Nature Communications 540 2021 12:1, 12, 1–8, https://doi.org/10.1038/s41467-021-25699-w, 2021.

Hillebrand, H. and Azovsky, A. I.: Body size determines the strength of the latitudinal diversity gradient, Ecography, 24, 251–256, https://doi.org/10.1034/J.1600-0587.2001.240302.X, 2001.

Hirata, T., Aiken, J., Hardman-Mountford, N., Smyth, T., and Barlow, R.: An absorption model to determine phytoplankton size classes from satellite ocean colour, Remote Sensing of Environment, 112, 3153–3159, https://doi.org/10.1016/J.RSE.2008.03.011, 2008.

545 Hirata, T., Hardman-Mountford, N. J., Brewin, R. J. W., Aiken, J., Barlow, R., Suzuki, K., Isada, T., Howell, E., Hashioka, T., Noguchi-Aita, M., and Yamanaka, Y.: Synoptic relationships between surface Chlorophyll-a and diagnostic pigments specific to phytoplankton functional types, Biogeosciences, 8, 311–327, https://doi.org/10.5194/bg-8-311-2011, 2011.

Hood, R. R., Laws, E. A., Armstrong, R. A., Bates, N. R., Brown, C. W., Carlson, C. A., Chai, F., Doney, S. C., Falkowski, P. G., Feely, R. A., Friedrichs, M. A., Landry, M. R., Keith Moore, J., Nelson, D. M., Richardson, T. L., Salihoglu, B., Schartau, M., Toole, D. A.,

550   and Wiggert, J. D.: Pelagic functional group modeling: Progress, challenges and prospects, Deep Sea Research Part II: Topical Studies in Oceanography, 53, 459–512, https://doi.org/10.1016/J.DSR2.2006.01.025, 2006.

Ibarbalz, F. M., Henry, N., Brandão, M. C., Martini, S., Busseni, G., Byrne, H., Coelho, L. P., Endo, H., Gasol, J. M., Gregory, A. C., Mahé, F., Rigonato, J., Royo-Llonch, M., Salazar, G., Sanz-Sáez, I., Scalco, E., Soviadan, D., Zayed, A. A., Zingone, A., Labadie, K., Ferland, J., Marec, C., Kandels, S., Picheral, M., Dimier, C., Poulain, J., Pisarev, S., Carmichael, M., Pesant, S., Acinas, S. G., Babin, M., Bork, P.,
555   Boss, E., Bowler, C., Cochrane, G., de Vargas, C., Follows, M., Gorsky, G., Grimsley, N., Guidi, L., Hingamp, P., Iudicone, D., Jaillon, O., Karp-Boss, L., Karsenti, E., Not, F., Ogata, H., Poulton, N., Raes, J., Sardet, C., Speich, S., Stemmann, L., Sullivan, M. B., Sunagawa, S., Wincker, P., Pelletier, E., Bopp, L., Lombard, F., and Zinger, L.: Global Trends in Marine Plankton Diversity across Kingdoms of Life, Cell, 179, 1084–1097.e21, https://doi.org/10.1016/J.CELL.2019.10.008, 2019.

Iglesias-Rodríguez, M. D., Brown, C. W., Doney, S. C., Kleypas, J., Kolber, D., Kolber, Z., Hayes, P. K., and Falkowski, P. G.: Representing
560   key phytoplankton functional groups in ocean carbon cycle models: Coccolithophorids, Global Biogeochemical Cycles, 16, 47–1–47–20, https://doi.org/10.1029/2001GB001454, 2002.

Irigoien, X., Hulsman, J., and Harris, R. P.: Global biodiversity patterns of marine phytoplankton and zooplankton, Nature 2004 429:6994, 429, 863–867, https://doi.org/10.1038/nature02593, 2004.

Jouini, M., Lévy, M., Crépon, M., and Thiria, S.: Reconstruction of satellite chlorophyll images under heavy cloud coverage using a neural
565   classification method, Remote Sensing of Environment, 131, 232–246, https://doi.org/10.1016/j.rse.2012.11.025, 2013.

Le Quéré, C., Harrison, S. P., Colin Prentice, I., Buitenhuis, E. T., Aumont, O., Bopp, L., Claustre, H., Cotrim Da Cunha, L., Geider, R., Giraud, X., Klaas, C., Kohfeld, K. E., Legendre, L., Manizza, M., Platt, T., Rivkin, R. B., Sathyendranath, S., Uitz, J., Watson, A. J., and Wolf-Gladrow, D.: Ecosystem dynamics based on plankton functional types for global ocean biogeochemistry models, Global Change Biology, 0, 051013014052 005–???, https://doi.org/10.1111/j.1365-2486.2005.1004.x, 2005.

570   Luo, Y.-W., Doney, S. C., Anderson, L. A., Benavides, M., Berman-Frank, I., Bode, A., Bonnet, S., Boström, K. H., Böttjer, D., Capone, D. G., Carpenter, E. J., Chen, Y. L., Church, M. J., Dore, J. E., Falcón, L. I., Fernández, A., Foster, R. A., Furuya, K., Gómez, F., Gundersen, K., Hynes, A. M., Karl, D. M., Kitajima, S., Langlois, R. J., LaRoche, J., Letelier, R. M., Marañón, E., McGillicuddy, D. J., Moisander, P. H., Moore, C. M., Mouriño-Carballido, B., Mulholland, M. R., Needoba, J. A., Orcutt, K. M., Poulton, A. J., Rahav, E., Raimbault, P., Rees, A. P., Riemann, L., Shiozaki, T., Subramaniam, A., Tyrrell, T., Turk-Kubo, K. A., Varela, M., Villareal, T. A., Webb,
575   E. A., White, A. E., Wu, J., and Zehr, J. P.: Database of diazotrophs in global ocean: abundance, biomass and nitrogen fixation rates, Earth System Science Data, 4, 47–73, https://doi.org/10.5194/essd-4-47-2012, 2012.

Mitchell, B. G., Brody, E. A., Holm-Hansen, O., McClain, C., and Bishop, J.: Light limitation of phytoplankton biomass and macronutrient utilization in the Southern Ocean, Limnology and Oceanography, 36, 1662–1677, https://doi.org/10.4319/lo.1991.36.8.1662, 1991.

O'Reilly, J. E., Maritorena, S., Mitchell, B. G., Siegel, D. a., Carder, K. L., Garver, S. a., Kahru, M., and McClain, C.: Ocean color chlorophyll
580   algorithms for SeaWiFS, Journal of Geophysical Research, 103, 24 937, https://doi.org/10.1029/98JC02160, 1998.

Organelli, E., Bricaud, A., Antoine, D., and Uitz, J.: Multivariate approach for the retrieval of phytoplankton size structure from measured light absorption spectra in the Mediterranean Sea (BOUSSOLE site), Applied Optics, 52, 2257, https://doi.org/10.1364/AO.52.002257, 2013.

Peloquin, J., Swan, C., Gruber, N., Vogt, M., Claustre, H., Ras, J., Uitz, J., Barlow, R., Behrenfeld, M., Bidigare, R., Dierssen, H., Ditullio,
585   G., Fernandez, E., Gallienne, C., Gibb, S., Goericke, R., Harding, L., Head, E., Holligan, P., Hooker, S., Karl, D., Landry, M., Letelier, R., Llewellyn, C. A., Lomas, M., Lucas, M., Mannino, A., Marty, J.-c., Mitchell, B. G., Muller-Karger, F., Nelson, N., Prezelin, B., Repeta, D., Smith Jr, W. O., Smythe-Wright, D., Stumpf, R., Subramaniam, A., Suzuki, K., Trees, C., Vernet, M., Wasmund, N., and Wright,

S.: The MAREDAT global database of high performance liquid chromatography marine pigment measurements, Earth Syst. Sci. Data, 5, 109–123, https://doi.org/10.5194/essd-5-109-2013, 2013.

590 Pereira, H. M., Ferrier, S., Walters, M., Geller, G. N., Jongman, R. H., Scholes, R. J., Bruford, M. W., Brummitt, N., Butchart, S. H., Cardoso, A. C., Coops, N. C., Dulloo, E., Faith, D. P., Freyhof, J., Gregory, R. D., Heip, C., Höft, R., Hurtt, G., Jetz, W., Karp, D. S., McGeoch, M. A., Obura, D., Onoda, Y., Pettorelli, N., Reyers, B., Sayre, R., Scharle-mann, J. P., Stuart, S. N., Turak, E., Walpole, M., and Wegmann, M.: Essential biodiversity variables, Science, 339, 277–278, https://doi.org/10.1126/SCIENCE.1229931/SUPPL_FILE/1229931.PEREIRA.SM.PDF, 2013.

595 Pesant, S., Not, F., Picheral, M., Kandels-Lewis, S., Le Bescot, N., Gorsky, G., Iudicone, D., Karsenti, E., Speich, S., Trouble, R., Dimier, C., and Searson, S.: Open science resources for the discovery and analysis of Tara Oceans data, Scientific Data, 2, https://doi.org/10.1038/SDATA.2015.23, 2015.

Pierella Karlusich, J. J., Ibarbalz, F. M., and Bowler, C.: Phytoplankton in the Tara Ocean, https://doi.org/10.1146/annurev-marine-010419-010706, 12, 233–265, https://doi.org/10.1146/ANNUREV-MARINE-010419-010706, 2020.

600 Pierella Karlusich, J. J., Pelletier, E., Zinger, L., Lombard, F., Zingone, A., Colin, S., Gasol, J. M., Dorrell, R. G., Henry, N., Scalco, E., Acinas, S. G., Wincker, P., de Vargas, C., and Bowler, C.: A robust approach to estimate relative phytoplankton cell abundances from metagenomes, Molecular Ecology Resources, 00, 1–25, https://doi.org/10.1111/1755-0998.13592, 2022.

Powell, M. G. and Glazier, D. S.: Asymmetric geographic range expansion explains the latitudinal diversity gradients of four major taxa of marine plankton, Paleobiology, 43, 196–208, https://doi.org/10.1017/PAB.2016.38, 2017.

605 Raven, J.: The twelfth Tansley Lecture. Small is beautiful: the picophytoplankton, Functional ecology, 12, 503–513, 1998.

Reygondeau, G., Irisson, J.-O., Ayata, S. D., Gasparini, S., Benedetti, F., Albouy, C., Hattab, T., Guieu, C., and Koubbi., P.: Definition of the Mediterranean Eco-regions and Maps of Potential Pressures in These Eco-regions, Tech. rep., Perseus Deliverable 1, http://www.perseus-net.eu/assets/media/PDF/deliverables/3336.6_Final.pdf, 2014.

Richardson, A. J., Risien, C., and Shillington, F. A.: Using self-organizing maps to identify patterns in satellite imagery, Progress in Oceanog-610 raphy, 59, 223–239, https://doi.org/10.1016/j.pocean.2003.07.006, 2003.

Righetti, D., Vogt, M., Gruber, N., Psomas, A., and Zimmermann, N. E.: Global pattern of phytoplank-ton diversity driven by temperature and environmental variability, Science Advances, 5, 6253–6268, https://doi.org/10.1126/SCIADV.AAU6253/SUPPL_FILE/AAU6253_SM.PDF, 2019.

Rodríguez-Ramos, T., Marañón, E., and Cermeño, P.: Marine nano- and microphytoplankton diversity: redrawing global patterns from 615 sampling-standardized data, Global Ecology and Biogeography, 24, 527–538, https://doi.org/10.1111/GEB.12274, 2015.

Rossi, V., Ser-Giacomi, E., Lõpez, C., and Hernández-García, E.: Hydrodynamic provinces and oceanic connectivity from a transport network help designing marine reserves, Geophysical Research Letters, 41, 2883–2891, https://doi.org/10.1002/2014GL059540, 2014.

Sarzeaud, O. and Stephan, Y.: Data interpolation using Kohonen networks, Proceedings of the International Joint Conference on Neural Networks, 6, 197–202, 2000.

620 Sathyendranath, S., Aiken, J., Alvain, S., Barlow, R., Bouman, H., Bracher, A., Brewin, R., Bricaud, A., Brown, C. W., Ciotti, A. M., Clementson, L. A., Craig, S. E., Devred, E., Hardman-Mountford, N., Hirata, T., Hu, C., Kostadinov, T. S., Lavender, S., Loisel, H., Moore, T. S., Morales, J., Mouw, C. B., Nair, A., Raitsos, D., Roesler, C., Shutler, J. D., Sosik, H. M., Soto, I., Stuart, V., Subramaniam, A., and Uitz, J.: Phytoplankton functional types from Space, International Ocean-Colour Coordinating Group, Dartmouth, Nova Scotia, B2Y 4A2, Canada., ioccg; 15 edn., https://epic.awi.de/id/eprint/36000/, 2014.

625 Sawadogo, S., Brajard, J., Niang, A., Lathuiliere, C., Crepon, M., and Thiria, S.: Analysis of the Senegalo-Mauritanian upwelling by processing satellite remote sensing observations with topological maps., in: 2009 International Joint Conference on Neural Networks, pp. 2826–2832, IEEE, https://doi.org/10.1109/IJCNN.2009.5178623, 2009.

Smith, V. H.: Microbial diversity–productivity relationships in aquatic ecosystems, FEMS Microbiology Ecology, 62, 181–186, https://doi.org/10.1111/J.1574-6941.2007.00381.X, 2007.

630 Sommeria-Klein, G., Watteaux, R., Ibarbalz, F. M., Karlusich, J. J. P., Iudicone, D., Bowler, C., and Morlon, H.: Global drivers of eukaryotic plankton biogeography in the sunlit ocean, Science, 374, 594–599, https://doi.org/10.1126/SCIENCE.ABB3717/SUPPL_FILE/SCIENCE.ABB3717_MDAR_REPRODUCIBILITY_CHECKLIST.PDF, 2021.

Soppa, M. A., Hirata, T., Silva, B., Dinter, T., Peeken, I., Wiegmann, S., and Bracher, A.: Global retrieval of diatom abundance based on
635 phytoplankton pigments and satellite data, Remote Sensing, 6, 10 089–10 106, https://doi.org/10.3390/rs61010089, 2014.

Tara Ocean Foundation, Tara Oceans, E. M. B. L. E. . E. M. B. R. C. R. I. C. E.: Priorities for ocean microbiome research, Nature Microbiology, 7, 937–947, 2022.

Tilman, D., Isbell, F., and Cowles, J. M.: Biodiversity and Ecosystem Functioning, Annu. Rev. Ecol. Evol. Syst, 45, 471–493, https://doi.org/10.1146/annurev-ecolsys-120213-091917, 2014.

640 Uitz, J., Claustre, H., Morel, A., and Hooker, S. B.: Vertical distribution of phytoplankton communities in open ocean: An assessment based on surface chlorophyll, J. Geophys. Res., 111, C08 005, https://doi.org/10.1029/2005jc003207, 2006.

Vidussi, F., Claustre, H., Manca, B. B., Luchetta, A., and Marty, J.-C.: Phytoplankton pigment distribution in relation to upper thermocline circulation in the eastern Mediterranean Sea during winter, Journal of Geophysical Research: Oceans, 106, 19 939–19 956, https://doi.org/10.1029/1999JC000308, 2001.

645 Werdell, P. J. and Bailey, S. W.: An improved in-situ bio-optical data set for ocean color algorithm development and satellite data product validation, Remote Sensing of Environment, 98, 122–140, https://doi.org/10.1016/j.rse.2005.07.001, 2005.

Wright, S. W., van den Enden, R. L., Pearce, I., Davidson, A. T., Scott, F. J., and Westwood, K. J.: Phytoplankton community structure and stocks in the Southern Ocean (30–80 E) determined by CHEMTAX analysis of HPLC pigment signatures, Deep Sea Research Part II: Topical Studies in Oceanography, 57, 758–778, 2010.

650 Xi, H., Hieronymi, M., Röttgers, R., Krasemann, H., and Qiu, Z.: Hyperspectral differentiation of phytoplankton taxonomic groups: a comparison between using remote sensing reflectance and absorption spectra, Remote Sensing, 7, 14 781–14 805, 2015.

Xi, H., Losa, S. N., Mangin, A., Soppa, M. A., Garnesson, P., Demaria, J., Liu, Y., D'Andon, O. H. F., and Bracher, A.: Global retrieval of phytoplankton functional types based on empirical orthogonal functions using CMEMS GlobColour merged products and further extension to OLCI data, Remote Sensing of Environment, 240, 111 704, https://doi.org/10.1016/J.RSE.2020.111704, 2020.